

Compact and highly-efficient polarization independent vertical resonant couplers for active-passive monolithic integration

Marko Galarza,^{1,*} Dries Van Thourhout,² Roel Baets,² and Manuel Lopez-Amo¹

¹Department of Electrical and Electronic Engineering, Public University of Navarre, Campus Arrosadía, 31006 Pamplona, Spain

²Department of Information Technology, University of Ghent, St.-Pietersnieuwstraat 41, B-9000 Ghent, Belgium

*Corresponding author: marko.galarza@unavarra.es

Abstract: Compact low-loss polarization independent vertical coupling between a 1.55 μm InGaAsP bulk active waveguide and a passive waveguide based on bimodal interference is presented. Simulation results show low coupling loss (<0.1 dB) over coupler lengths more than 5 times shorter than using the adiabatic design. The concept avoids submicron photolithographic features and shows acceptable fabrication tolerances.

©2008 Optical Society of America

OCIS codes: (130.0130) Integrated optics; (130.2790) Guided waves; (130.1750) Components.

References and links

1. E. Tangdiongga, Y. Liu, J. H. Den Besten, M. van Geemert, T. Van Dongen, J. J. M. Binsma, H. De Waardt, G. D. Khoe, M. K. Smit, and H. J. S. Dorren, "Monolithically integrated 80-Gb/s AWG-based all-optical wavelength converter," *IEEE Photon. Technol. Lett.* **18**, 1627-1629 (2006).
2. T. Van Caenegem, D. Van Thourhout, M. Galarza, S. Verstuyft, I. Moerman, P. Van Daele, R. Baets, P. Demeester, C. G. P. Herben, X. J. M. Leijtens, and M. K. Smit, "Monolithically integrated multi-wavelength laser by selective area growth with metal organic vapour phase epitaxy," *Electron. Lett.* **37**, 296-298 (2001).
3. J. Dubowski, Y. Feng, P. Poole, M. Buchanan, S. Poirier, J. Genest, and V. Aimez, "Monolithic multiple wavelength ridge waveguide laser array fabricated by Nd:YAG laser induced quantum well intermixing," *J. Vac. Sci. Technol. A* **20**, 1426-1429 (2002).
4. V. Lal, M. L. Masanovic, J. A. Summers, G. Fish, and D. J. Blumenthal, "Monolithic wavelength converters for high-speed packet-switched optical networks," *IEEE J. Sel. Top. Quantum Electron.* **13**, 49-57 (2007).
5. Y. Suematsu, M. Yamada, and K. Kayashi, "Integrated twin-guide AlGaAs laser with multiheterostructure," *IEEE J. Quantum Electron.* **QE-11**, 457-460 (1975).
6. V. Vusirikala, S. S. Saini, R. E. Bartolo, S. Argawala, R. D. Whaley, F. G. Johnson, D. R. Stone, and M. Dagenais, "1.55- μm InGaAsP-InP Laser Arrays with Integrated-Mode Expanders Fabricated Using a Single Epitaxial Growth," *IEEE J. Sel. Top. Quantum Electron.* **3**, 1332-1343 (1997).
7. S. S. Saini, Z. Dilli, F. G. Johnson, H. Shen, W. Zhou, and M. Dagenais, "Taper length variation in passive active resonant coupler PARC platform," in *Integrated Photonics Research*, Vol. **46** of OSA Trends in Optics and Photonics Optical Society of America (Washington, D.C., 1976), paper IThG3.
8. M. K. Chin and C. W. Lee, "Polarization-independent vertical coupler for photonics integration," *Opt. Express* **12**, 117-123 (2004).
9. P. V. Studenkov, M. R. Gokhale, and S. R. Forrest, "Efficient coupling in integrated twin-waveguide lasers using waveguide tapers," *IEEE Photon. Technol. Lett.* **11**, 1096-1098 (1999).
10. V. M. Menon, F. Xia, and S. R. Forrest, "Photonic integration using asymmetric twin-waveguide technology: Part II-Devices," *IEEE J. Sel. Top. Quantum Electron.* **11**, 30-42 (2005).
11. J. D. Love, W. M. Henry, W. J. Stewart, R. J. Black, S. Lacroix, and F. Gonthier, "Tapered single-mode fibers and devices. Part I: Adiabaticity criteria," *IEEE Proc.-J* **138**, 343-354 (1991).
12. M. Galarza, K. De Mesel, R. Baets, A. Martinez, C. Aramburu, and M. Lopez-Amo, "Compact spot-size converters with fiber-matched antiresonant reflecting optical waveguide," *Appl. Opt.* **42**, 4841-4846 (2003).
13. The European FP6 Network of Excellence ePIXnet: <http://www.epixnet.org>.
14. Fimmwave/Fimmprop, Photon Design; <http://www.photond.com>.
15. OptiBPM, Optiwave Corporation; <http://www.optiwave.com>.

1. Introduction

The route forward for photonics is, just as it was for electronics, the integration of multifunctional and highly optimized devices in a single chip in order to realize high

performance components required in next generation lightwave communication systems. Planar monolithic integration is the way to integrate as much as possible the different active and passive functionalities of the opto-electronical component on a single substrate, resulting in small and compact units. It offers higher reliability due to the elimination of mechanical movements among the elements and a significant reduction in production cost due to the batch processing of wafers.

Over the past years several active-passive integration techniques have been developed. Butt-joint regrowth [1], selective area growth [2], quantum well intermixing [3] and offset quantum wells [4] are complex and expensive technologies that result in high cost devices and/or low yields. Suematsu, et al. [5] proposed the integrated twin-guide structure, where the active and passive functions are separated into two different vertically displaced waveguides, eliminating the need for material regrowth or any post-growth processing. Nevertheless, both waveguides have to be phase matched to transfer power by resonant coupling of the two supermodes, and a compromise in the device performance has to be defined because the active and passive functionalities cannot be optimized separately.

In [6-10] the authors propose the use of asymmetric twin-waveguides (ATG) with taper couplers. They utilize an active waveguide with a higher effective index than the passive waveguide, making them strongly asymmetric. Under this condition the even mode dominates in the active devices due to its larger gain and the odd mode is never excited, allowing the independent optimization of the active devices. The power transfer to the passive waveguide is realized using a lateral tapering of the active waveguide. However, although the authors in [6-9] suggest there is a resonant point where the effective indices of the two guides are matched, they do not describe the underlying physics governing the power transfer and it is not clear the power exchange between the modes supported by the structure. Fully adiabatic approaches [10] imply rather long designs ($\sim 150 \mu\text{m}$) and sub-micron final taper tips ($\sim 0.5 \mu\text{m}$), which are difficult to achieve by standard lithography.

In this paper, we propose an approach for the monolithic integration of InGaAsP active and passive waveguides fully based on bimodal interference between the two supermodes supported by the vertical structure formed by the active waveguide and the passive waveguide. This concept provides higher performance than the devices proposed so far, over a considerably shorter length and without the need of sub-micron lithography. In Section 2 we present the concept for fully resonant couplers. In Section 3 we outline the waveguide structure and coupler design. In Section 4 we present the simulation results on mode transformation efficiency, as well as a tolerance analysis for width, etching depth and alignment variations. Finally, in Section 5 we provide the summary and conclusions.

2. Concept

Figure 1(a) shows a simplified two dimensional representation of the adiabatic mode transformation produced in a tapered ATG (the lateral tapering of the real tapers is shown as a vertical tapering in the figure for clarity purposes). The mode generated in the upper active waveguide is in fact the even supermode ψ_e of the complete structure formed by the active and the passive waveguides. In an adiabatic taper all the power remains in this mode while it is being transformed (see Fig. 1(a)). The odd supermode ψ_o supported by the structure is not excited in the adiabatic regime and when the tapered upper rib waveguide reaches cut-off due to the tapering, this mode ψ_o is not a guided mode any more and becomes a radiation mode.

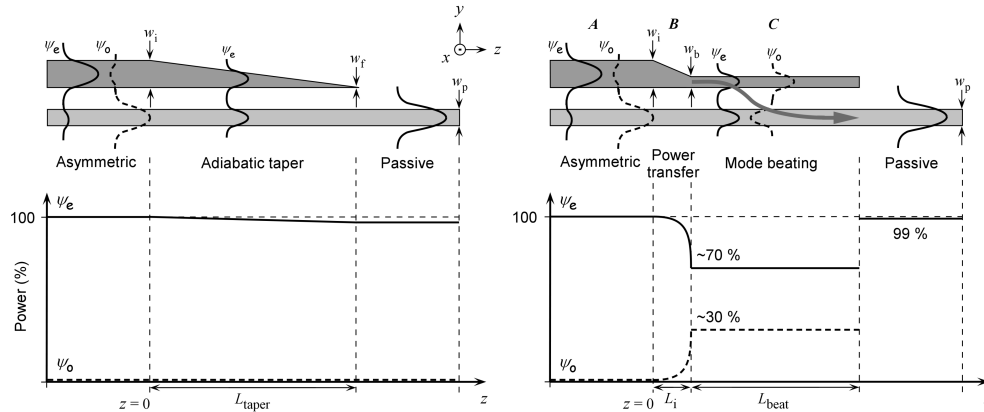


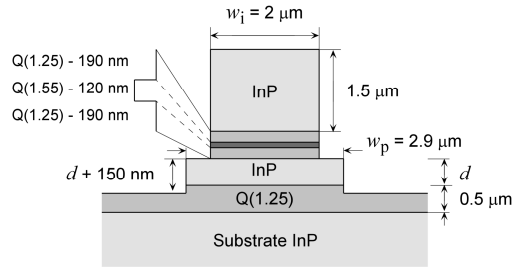
Fig. 1. (a). In the adiabatic mode transformation concept, the even supermode ψ_e of the taper is smoothly transformed into the passive mode without losing any power. (b) In the bimodal interference taper concept the fundamental supermode ψ_e transfers power to the odd one ψ_o , and the interference between them couples the field in the passive waveguide.

The mode transformation concept based on the bimodal interference between the two guided supermodes of the twin structure is schematically shown in Fig. 1(b). In region A all the power is carried by the even mode ψ_e . The odd mode ψ_o is also shown, although it is not excited in the active section. In region B, an abrupt tapering of the waveguide provokes the transfer of part of the power from the fundamental even mode ψ_e to the odd mode ψ_o of the structure. In the straight section of region C the two modes propagate without loss and interfere. At the beginning of region C the field is concentrated in the upper active waveguide, but when the supermodes reach the beating length (when their phase difference $\Delta\phi = \pi$), the power is concentrated in the lower passive waveguide and matches perfectly the mode of the individual passive waveguide.

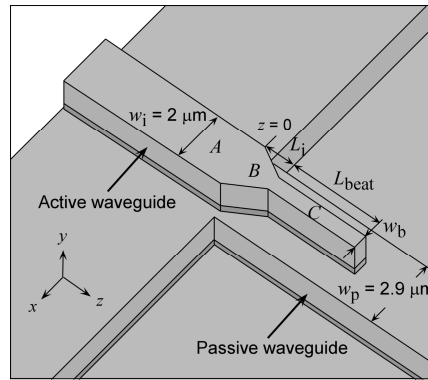
The technique used to transfer power from the even eigenmode ψ_e to the odd one ψ_o can be understood by coupled-mode theory. In the classical equation of coupled-mode theory it is assumed that the transfer of power from the fundamental mode of a non-adiabatic taper will be predominantly to the higher order mode with a propagation constant closest to that of the fundamental mode [11]. In the case we are considering this power-receiving mode is the odd supermode ψ_o . Therefore, using slopes that are beyond the adiabatic critical slope in region B we force the power transfer between the fundamental even mode ψ_e and the odd mode ψ_o . However, if the slope of this tapering is too sharp, we will have undesired radiation to higher-order modes that decrease the coupler efficiency [12]; thus a compromise between intermodal power transfer and coupler efficiency has to be found.

3. Design

The transverse structure of the proposed vertical coupler is shown in Fig. 2(a) and is the same waveguide structure as developed for the Joint European Platform for InP-based Photonic Integrated Components and Circuits (JePPIX) within the European FP6 Network of Excellence ePIXnet [13]. The component consists of a 0.5- μm -thick InGaAsP layer (with a bandgap cutoff wavelength of $\lambda_g = 1.25 \mu\text{m}$), an InP separation layer of thickness d , and an active waveguide containing a bulk core of 120-nm-thick quaternary material for emission at 1.55 μm (Q1.55) surrounded by 190-nm-thick undoped confining layers having the same composition as the passive core (Q1.25). The three dimensional (3D) schematic of the ATG laser with resonant taper coupler is shown in Fig. 2(b). The width of the active and passive waveguide is 2 μm and 2.9 μm , respectively.



(a)



(b)

Fig. 2. (a). Schematic drawing of the ATG showing the tapered upper active rib and the underlying passive waveguide. (b) Schematic diagram of the tapering shape of the resonant coupler based on bimodal interference.

A commercial 3D complex mode solver (Fimmwave) and a fully vectorial 3D propagation tool (Fimmprop) [14] are used to design and analyze the proposed coupler. The most important and critical section to be designed is the power transfer section *B*, defined by w_i , w_b and L_i . The initial width w_i is defined by the width of the active section, which is $2 \mu\text{m}$. Efficient and stable modal power transfer efficiency is observed in region *B*, if L_i is maintained in the range 2-10 μm . Thus, we choose a safe length L_i of $5 \mu\text{m}$.

The resonant width w_b of the upper guide for which the effective indices of the two guides are matched is slightly different for both TE and TM transverse polarizations. Figure 3 shows the effective indexes of the upper and the lower waveguides as a function of the width for $d = 0.5 \mu\text{m}$. The width of the tapered upper waveguide at which the effective index crosses that of the lower waveguide is defined as the resonant width w_b . The design of w_b and L_{beat} is an iterative process, starting with the average resonant width while varying the length to determine the optimum value for maximum average transfer efficiency for both polarizations.

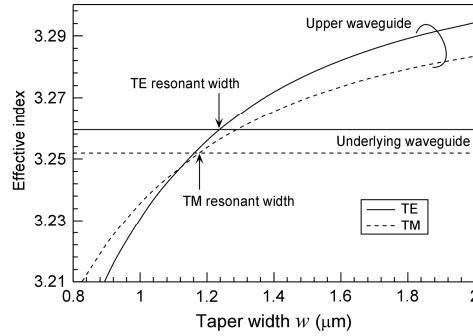


Fig. 3. Effective indexes of the coupled waveguide for TE and TM modes at various taper widths.

Table 1 shows the calculated optimum parameters for several values of the intermediate InP layer thickness d (0.3, 0.5 and 0.7 μm) and for polarization independent transformation. A fully numerical simulation method has been employed to strength the proposed designs. Using a commercial 3D beam propagation method software [15] for verification, identical results as the ones provided by the mode propagation tool were obtained.

Table 1. Design parameters for three polarization independent resonant couplers.

d	0.3	0.5	0.7
L_i	5	5	5
w_b	1.04	1.18	1.23
L_{beat}	19	44	85

Figure 4 shows the top (x - z) and lateral (y - z) plot of the total field (including reflections) transforming along the coupler. TE polarization and a thickness of the separation InP layer $d = 0.5 \mu\text{m}$ have been considered for propagation. Very good field transformation is confirmed between both vertical waveguides and no coupling to radiation modes is observed.

The upper row of Fig. 5 shows the field distribution at three points in the coupler during propagation. We observe how the field generated in the active waveguide and entering region B keeps its shape in the upper waveguide at the end of the power transfer section B . This field distribution excites very efficiently the two guided supermodes in the beating section C in a rate of 70:30, coupling less than 0.05 dB to radiation modes (see lower row of Fig. 5). As the two supermodes propagate in the straight section C , they interfere and for the correct coupling length result in a field distribution that matches the passive mode, losing only 0.05 dB more.

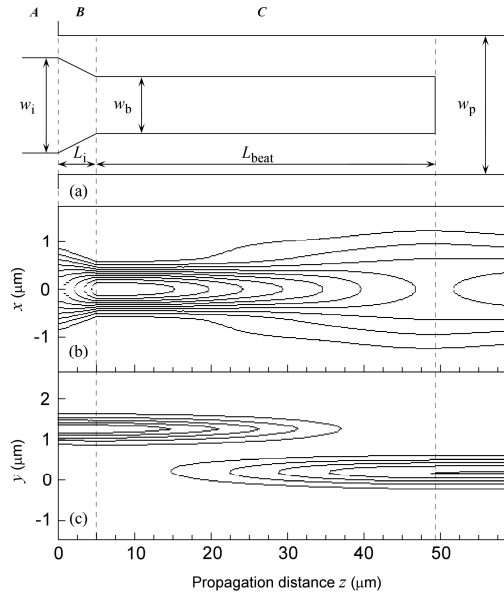


Fig. 4. Average TE field distribution as a function of the distance for the taper shape shown in (a). (b) Top view or x - z cut, (c) lateral view or y - z cut. Fimmwave was used for propagation.

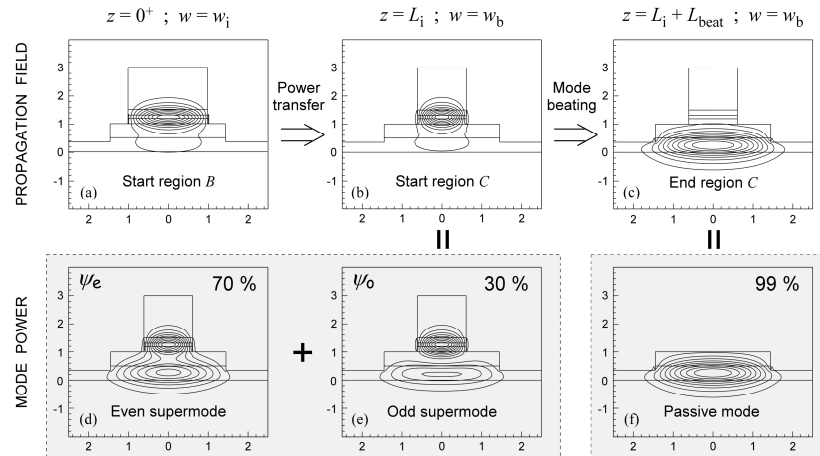


Fig. 5. (a). (b) (c) Transversal field distributions for a propagation run. (d). (e). (f) Modal field distributions at points (b) and (c). TE polarization was used in the simulation run. More insight is detailed in the text.

4. Simulation results

Table 2 shows all simulation results for the three different designs described in Table 1 ($d = 0.3, 0.5$ and $0.7 \mu\text{m}$), and for both polarizations TE and TM. The presence of the vertically stacked passive core close to the active waveguide in the ATG structure alters the shape of its fundamental mode spreading it and reducing the confinement factor η in the bulk quaternary Q1.55 material. The confinement values calculated in Table 2 have to be compared to the confinement factor of the individual active waveguide, which is 0.264 and 0.208 for TE and TM, respectively. It is obvious that the smaller the thickness of the intermediate layer d , the smaller the confinement factor η . Nevertheless, the reduction is smaller than a 13% for TE

polarized mode light and $d = 0.3 \mu\text{m}$, and less than 18% for TM polarized mode in the same case, keeping practical values for efficient gain. Moreover, the width w_i of the active waveguide is a free parameter which could be augmented to increase the confinement factor with negligible effect in the performance of the coupler. This would be possible since the modal power transfer of region B is mainly produced in the narrower part of the taper.

Table 2. Simulation results for the three designs corresponding to different InP separation layer thicknesses d .

d	TE			TM			units
	0.3	0.5	0.7	0.3	0.5	0.7	μm
η	0.230	0.255	0.259	0.172	0.199	0.202	–
κ	86:14	95:05	99:01	82:18	93:07	98:02	–
M	65:34	59:41	57:42	80:19	76:23	75:24	–
T	98	96	90	98	95	90	%
L_{total}	24	49	90	24	49	90	μm
w_b	1.05	1.16	1.23	1.05	1.16	1.23	μm
L_{adia}	115	195	255	140	245	272	μm
w_f	0.7	0.8	0.8	0.7	0.8	0.8	μm
Δw	± 125	± 73	± 35	± 125	± 73	± 35	nm
Δe	$>\pm 200$	nm					
Δg	$>\pm 300$	nm					

The asymmetry κ of the ATG is defined as the fraction of power confined in each waveguide. We observe in Table 2 that for a separation layer of $0.7 \mu\text{m}$ the asymmetry is very high: 99:01 for TE polarized light, and 98:02 for TM polarized light, making this configuration suitable for devices requiring high confinement in the active layers. The asymmetry is reduced to 86:14 and 82:18, respectively, for $d = 0.3 \mu\text{m}$.

The parameter M is defined as the fraction of the power transferred from the fundamental even mode ψ_e to the odd mode ψ_o . We observe a smaller ratio for TM polarization due to its lower resonant width compared to TE polarization.

The parameter T states the coupling transformation efficiency in %. The polarization independent devices show efficiencies of 98, 96 and 90% for the three separation thicknesses respectively. Next in Table 2, are the total lengths L_{total} of the vertical couplers and, in spite of being redundant, the resonance widths w_i are also shown. The reason is to provide a clearer comparison with the lengths L_{adia} and minimum taper tips w_f that adiabatically designed tapers would need to reach the previously mentioned efficiencies. Length reduction ratios of 5.8 (140/24), 5, (245/49) and 3 (272/90) are obtained for the three InP layer thicknesses d : 0.3, 0.5 and $0.7 \mu\text{m}$, respectively. Figure 6 shows the efficiency of the resonant coupler compared to the efficiency of the adiabatic design as a function of the coupler total length for $d = 0.5 \mu\text{m}$. A fully periodic response is obtained for the bimodal coupler, whereas a smoother and continuously increasing efficiency is provided by the adiabatic tapers. Coupled mode theory has been used to design optimized adiabatic tapers [11]. Regarding the final taper tips w_f required in the adiabatic design, submicron features are needed in all three designs ($\leq 0.8 \mu\text{m}$). Contrary to that, since the proposed design is fully resonant, it abruptly cuts the upper waveguide at the beating length, when the width w_b is still higher than $1 \mu\text{m}$ (see Table 2).

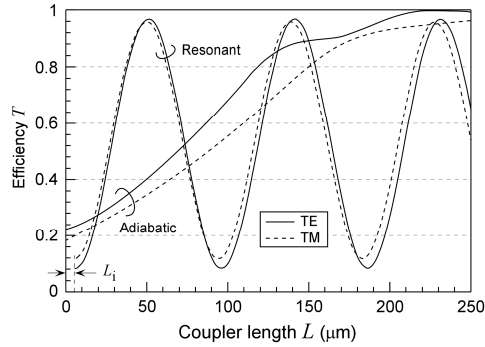


Fig. 6. Comparison of the taper efficiency as a function of length between the resonant coupling and adiabatic approaches.

We have performed a set of simulations to investigate the influence of changes in the width of the coupler Δw , the etching depth Δe and misalignments between both waveguides Δg , taking the efficiency T as a figure of merit. The last three rows in Table 2 show the 1-dB tolerance for these parameters. The resonant coupler concept performs strongly against etching depth and alignment variations, while being far more sensitive to width variations. Figure 7 plots the efficiency of the three designs as a function of changes in the width of the coupler waveguides. More relaxed values are obtained for thinner intermediate InP layers, allowing ± 125 nm for the $d = 0.3$ μm design.

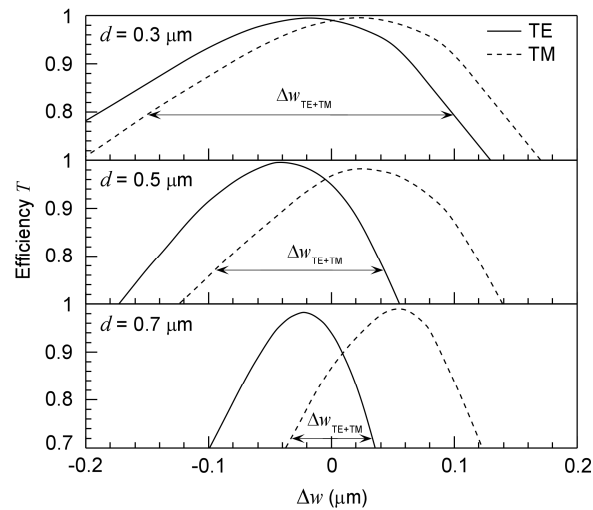


Fig. 7. Coupler efficiency as a function of width variations for three different separation layer thicknesses d and for both polarizations. $\Delta w = 0$ represents the polarization independent design, whereas the peaks would be chosen if only one polarization had to be optimized.

We observe a symmetrical increase of the efficiency around the optimum width w_b ; therefore, if instead of taking into account a polarization independent component, only one polarization had to be optimized, the efficiencies would easily reach 98% (less than 0.1 dB loss) and the width alignment tolerances would be somewhat higher: around ± 145 , ± 100 , ± 60 for 0.3, 0.5, 0.7 InP layer thicknesses, respectively.

5. Conclusion

In this work, we have presented highly efficient and polarization independent compact mode coupling between an active waveguide and a passive waveguide using fully bimodal interference. Modal transformation losses as low as 0.1 dB have been achieved using much shorter lengths than the adiabatic approach. The concept avoids submicron photolithographic features and show acceptable fabrication tolerances.

Acknowledgments

The authors would like to acknowledge Spanish Centro Interministerial de Ciencia y Tecnología for its support through the project CICYT-TEC2004-05936-C02-01/MIC, and for a Juan de la Cierva grant.